Optimization of Energy Harvesting MISO Communication Channels

Rajeev Gangula, *Student Member, IEEE*, David Gesbert, *Fellow, IEEE*, and Deniz Gündüz, *Senior Member, IEEE*

***Abstract*—Optimization of a point-to-point (p2p) multiple-input single-output (MISO) communication system is considered when both the transmitter (TX) and the receiver (RX) have energy harvesting (EH) capabilities. The RX is interested in feeding back the channel state information (CSI) to the TX to help improve the transmission rate. The objective is to maximize the throughput by a deadline, subject to the EH constraints at the TX and the RX. The throughput metric considered is an upper bound on the ergodic rate of the MISO channel with beamforming and limited feedback. Feedback bit allocation and transmission policies that maximize the upper bound on the ergodic rate are obtained. Tools from majorization theory are used to simplify the formulated optimization problems. Optimal policies obtained for the modified problem outperform the naive scheme in which no intelligent management of energy is performed.**

***Index Terms*—Energy harvesting, Limited feedback, MISO, Offline optimization.**

I. Introduction

Powering up terminals in communication networks by renewable ambient energy reduces the carbon footprint of the information and communication technologies, which can no longer be neglected with the exponential growth in the number of communication devices. Another advantage of EH technology is that, it increases the autonomy of battery-run communication devices. In traditional wireless networks nodes get their energy from the power grid by always or periodically connecting to it. While it is easy to connect the terminals to the grid in some networks, in others, such as sensor networks, it cannot be done once after the deployment. Therefore, in such networks a node's lifetime, and hence, the network lifetime, is constrained by the limited initial energy in the battery. Providing EH capabilities to the communication nodes is an attractive solution to the network lifetime problem [2]. An EH node can scavenge energy from the environment (typical sources are solar, wind, vibration, thermal, etc.) [3]. With EH nodes in the network, in principle, one can guarantee perpetual lifetime without the need of replacing batteries.

However, EH poses a new design challenge as the energy sources are typically sporadic and random. The main challenge lies in ensuring the Quality of Service (QoS) constraints of the network given the random and time varying energy sources. This calls for the intelligent management of various parameters involved in a communication system.

This work has been performed under the project E-CROPS, funded by CHIST-ERA. Part of this work has been published in [1].

R. Gangula and D. Gesbert are with the Mobile Communications department, EURECOM, France (email: {gangula,gesbert}@eurecom.fr).

D. Gunduz is with the Department of Electrical and Electronic Engineering, Imperial College London, UK (email: d.gunduz@imperial.ac.uk).

Recently, a significant number of papers have appeared studying the optimal transmission schemes for EH communication systems under different assumptions regarding the node's knowledge about the underlying EH process. Offline optimization framework deals with systems in which non-causal knowledge of the EH process is available. Within this frame work, optimal transmission schemes are studied for the p2p fading channel [4], broadcast channel [5], [6], [7] and relay channel [8], [9]. In [10] the processing energy cost is taken into account as well as the transmission energy; while a finite number of transmission rates is considered in [11]. See [12] for an extensive overview.

To the best of our knowledge, a common aspect of all prior works on EH communication networks is that the TX is assumed to have access to perfect CSI. Knowledge of the CSI at the TX is beneficial in designing the optimal channel adaptation techniques and the TX filters in multi-antenna systems. However, recent studies have demonstrated that, although feedback enhances the system performance, feedback resources, namely power and bandwidth, are limited, and must be spent wisely [13]. As a result, an important question arises: How do the EH constraints affect the design of feedback enabled wireless networks?

In this paper, we study the optimization of a feedback enabled EH MISO channel, where feedback is used to improve the rate through array gain. The system model and the main assumptions in this paper are given in Section III. In Section IV, we consider the optimization of the feedback policy under EH constraints at the RX, while the TX is assumed to have a constant power supply. The motivation is to address the following: In the case of EH, the available energy at the RX varies over time. Should the RX feedback same quality of CSI at all times? If so, can the CSI feedback quality be improved by using more bandwidth in the low energy scenario? In the second part of this paper (Section IV), we assume that both the TX and the RX harvest energy. In this case, the transmission power policy and the feedback policy are coupled, and need to be jointly optimized. Results from multivariate majorization theory are used to devise simple algorithms. We start by giving a brief preliminary description of majorization theory in Section II. Numerical results are presented in Section VI to validate the analysis. Finally, Section VII concludes the paper.

Notation: Boldface letters are used to denote matrices and vectors. The transpose and conjugate transpose of matrix $\mathbf{A}$ is denoted by $\mathbf{A}^{\mathrm{T}}$ and $\mathbf{A}^{\mathrm{H}}$, respectively. We use $d_{i,j}$ to denote the element at the i-th row and j-th column of matrix $\mathbf{D}$, and $|\mathcal{S}|$ to denote the cardinality of the set $\mathcal{S}$. The set of integers from m to n, $m < n$, is represented by $[m : n]$. The algorithm

with name "Algo" is represented as [output arguments]= Algo (input arguments). A circularly-symmetric complex Gaussian distributed random variable η with zero mean and variance σ^2 is denoted by $\eta \sim \mathcal{CN}(0, \sigma^2)$.

II. PRELIMINARIES

In this section, the basic notion of majorization is introduced and some important inequalities on convex functions that are used in this work are stated. The readers are referred to [14], [15] for a complete reference. We start by stating the Edmundson-Madansky's inequality.

Theorem 1: [14] If f is a convex function and x is a random variable with values in an interval $[a, b]$, then

$$\mathrm{E}\left[f\left(x\right)\right] \leq \frac{b-\mu}{b-a} f\left(a\right) + \frac{\mu-a}{b-a} f\left(b\right),$$

where μ is the mean of x.

Majorization theory formalizes the notion that the components of a vector $\boldsymbol{x}$ are "less spread out" than the components of a vector $\boldsymbol{y}$.

Definition 1: Let $\boldsymbol{x} = [x_1, \ldots, x_n], \boldsymbol{y} = [y_1, \ldots, y_n]$, $\boldsymbol{x}, \boldsymbol{y} \in \mathbb{R}^n$ and let $x_{(i)}$ denote the i-th largest component of $\boldsymbol{x}$. Then $\boldsymbol{x}$ is said to be *majorized* by $\boldsymbol{y}$, denoted by $\boldsymbol{x} \preceq \boldsymbol{y}$, if

$$\sum_{i=1}^{l} x_{(i)} \leq \sum_{i=1}^{l} y_{(i)}, \qquad \forall l \in [1 : n-1]$$
$$\sum_{i=1}^{n} x_{(i)} = \sum_{i=1}^{n} y_{(i)}.$$

Definition 2: [15, 2.A.1] An $n \times n$ matrix $\mathbf{D}$ with elements $d_{i,j}$ is *doubly stochastic* if

$$d_{i,j} \geq 0, \qquad \forall i, j \in [1 : n],$$
$$\sum_{i=1}^{n} d_{i,j} = 1, \ \forall j \in [1 : n] \ \text{ and } \ \sum_{j=1}^{n} d_{i,j} = 1, \ \forall i \in [1 : n].$$

Theorem 2: [15, 4.A.1, 4.B.1] For $\boldsymbol{x}, \boldsymbol{y} \in \mathbb{R}^n$, the following conditions are equivalent:

- $\boldsymbol{x} \preceq \boldsymbol{y}$.
- $\boldsymbol{x} = \boldsymbol{y}\mathbf{D}$ for some doubly stochastic matrix $\mathbf{D}$.
- For all continuous concave functions $g : \mathbb{R} \to \mathbb{R}$, $\sum_{i=1}^{n} g\left(x_i\right) \geq \sum_{i=1}^{n} g\left(y_i\right)$.

Definition 3: [15, 15.A.2] Let $\mathbf{X}$ and $\mathbf{Y}$ be $m \times n$ real matrices. Then $\mathbf{X}$ is said to be *majorized* by $\mathbf{Y}$, written $\mathbf{X} \preceq \mathbf{Y}$, if $\mathbf{X} = \mathbf{Y}\mathbf{D}$, where the $n \times n$ matrix $\mathbf{D}$ is doubly stochastic.

Theorem 3: [15, 15.A.4] Let $\mathbf{X}$ and $\mathbf{Y}$ be $m \times n$ real matrices. Then, $\mathbf{X} \preceq \mathbf{Y}$ if and only if

$$\sum_{i=1}^{n} g\left(\boldsymbol{x}_i^c\right) \geq \sum_{i=1}^{n} g\left(\boldsymbol{y}_i^c\right),$$

for all continuous concave functions $g : \mathbb{R}^m \to \mathbb{R}$; here $\boldsymbol{x}_i^c$ and $\boldsymbol{y}_i^c$ denote the i-th column vector of $\mathbf{X}$ and $\mathbf{Y}$, respectively.

III. SYSTEM MODEL

We consider a p2p MISO fading channel as shown in Fig. 1, where both the TX and the RX harvest energy from the environment. Each node is equipped with an individual energy buffer, i.e., a rechargeable battery, that can store the locally harvested energy.

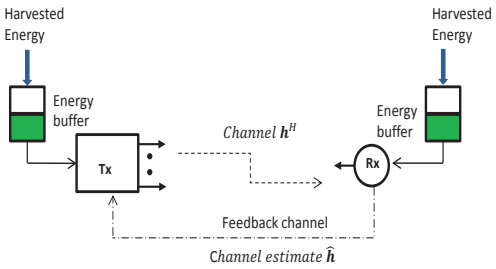

Figure 1. MISO channel with feedback, where both the TX and the RX harvest and store ambient energy.

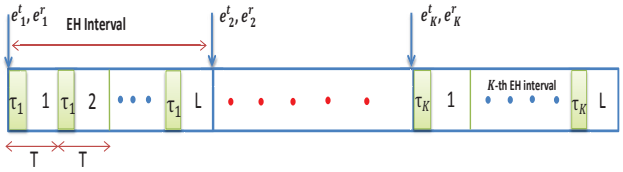

Figure 2. Energy harvesting time frame structure.

A. Energy Harvesting Model

The total observation time is divided into K equal length EH intervals. At the beginning of the k-th EH interval, $k \in [1 : K]$, energy packets of size e_k^t, e_k^r units arrive at the TX and the RX, respectively. At each node, this energy is first stored in an infinite size energy buffer, and used only for communication purposes, i.e., TX sending data, and the RX feeding back the CSI. We assume that all e_k^t, e_k^r's are known in advance by both terminals. This model is suitable for an EH system in which the profile of harvested energy either does not change over time, or it is time-varying but can be predicted accurately [12].

B. Communication System Model

Each EH interval consists of L data frames, each of length T channel uses. We assume a block fading channel model. The channel is constant during T channel uses of each frame, but changes in an independent and identically distributed (i.i.d.) fashion from one frame to another. The time frame structure is shown in Fig. 2. The TX has $M > 1$ antennas, while the RX has a single antenna. The received signal in a given channel use is given by

$$y = \boldsymbol{h}^{\mathrm{H}} \boldsymbol{w} s + \eta, \tag{1}$$

where $\boldsymbol{h} \in \mathbb{C}^{M \times 1}$ represents the vector of channel coefficients from TX to the RX with i.i.d. $\mathcal{CN}(0, 1)$ elements, $\boldsymbol{w} \in \mathbb{C}^{M \times 1}$ denotes the beamforming vector, the input symbol maximizing the achievable ergodic rate in the k-th EH interval is $s \sim \mathcal{CN}(0, p_k)$, and $\eta \sim \mathcal{CN}(0, 1)$ represents the noise at the RX.

C. Feedback Model

We assume that the RX perfectly estimates the channel state at the beginning of each data frame, and feeds back the quantized CSI to the TX within the same frame. In the k-th EH interval, the frame structure is as follows: The RX

in τ_k channel uses sends the CSI through a feedback channel (uplink) which is modeled as an additive white Gaussian noise (AWGN) channel. In the remaining $T-\tau_k$ channel uses, TX sends data to the RX (downlink) exploiting the obtained CSI. The feedback model represents the Time-Division Duplex (TDD) system in which uplink and downlink use the same band in a time-sharing fashion, but the communication devices are not self-calibrated, and hence, induce non-reciprocal effects [16], [17]. In the above model, although the feedback overhead incurs a cost in the downlink bandwidth, a similar trade-off in the resource allocation between the CSI feedback quality and uplink data rate also arise in a Frequency-Division Duplex (FDD) system [17]. Hence, the analytical results obtained in this paper are applicable in general settings, and for instance, can be used to address the trade-off between CSI quality and effective data rate in an FDD system.

In the k-th EH interval, quantization of the channel state is performed using a codebook $\mathcal{C}_k$ known at both the TX and RX. The receiver uses Random Vector Quantization (RVQ). The codebook consists of M-dimensional unit vectors $\mathcal{C}_k \triangleq \{\boldsymbol{f}_1, \ldots, \boldsymbol{f}_{2^{b_k}}\}$, where b_k is the number of bits used for quantization. The RX chooses the beamforming vector according to $\boldsymbol{w}_k = \arg\max_{\boldsymbol{f}\in\mathcal{C}_k} |\tilde{\boldsymbol{h}}^{\mathrm{H}}\boldsymbol{f}|^2$, where $\tilde{\boldsymbol{h}} \triangleq \frac{\boldsymbol{h}}{||\boldsymbol{h}||}$. We assume that the length of the EH interval is very large compared to the channel coherence time (i.e., L is very large). As a result, the achievable ergodic rate in the k-th EH interval is given by

$$R_k = \left(1-\frac{\tau_k}{T}\right) \mathrm{E}_{||\boldsymbol{h}||^2,\nu_k}\left[\log_2\left(1+\frac{p_k}{\left(1-\frac{\tau_k}{T}\right)}\|\boldsymbol{h}\|^2\nu_k\right)\right], \tag{2}$$

where $\nu_k = |\tilde{\boldsymbol{h}}^{\mathrm{H}}\boldsymbol{w}_k|^2$. Note that ν_k and $||\boldsymbol{h}||^2$ are independent [18]. By using the AWGN feedback channel model, the number of feedback bits b_k can be related to the energy used by the RX, q_k, and the number of channel uses τ_k as follows:

$$b_k = \tau_k \log_2\left(1+\frac{q_k}{\tau_k\sigma^2}\right), \tag{3}$$

where σ^2 is the noise variance in the uplink. For analytical tractability, we neglect the practical constraint that b_k should be an integer. Using the ergodic rate expression given in [18, Equation (27)] and (3), the ergodic rate $R_k \triangleq R(p_k, q_k, \tau_k)$ is found to be

$$R_k = \left(1-\frac{\tau_k}{T}\right)\log_2 e\left(e^{\rho_k}\sum_{l=0}^{M-1}E_{l+1}(\rho_k) - \int_{\nu_k=0}^{1}\left(1-(1-\nu_k)^{M-1}\right)^{N_k}\frac{M}{\nu_k}e^{\left(\frac{\rho_k}{\nu_k}\right)}E_{M+1}\left(\frac{\rho_k}{\nu_k}\right)d\nu_k\right) \tag{4}$$

where $\rho_k = \left(\frac{1-\frac{\tau_k}{T}}{p_k}\right)$, $N_k = \left(1+\frac{q_k}{\tau_k\sigma^2}\right)^{\tau_k}$, and $E_n(x) \triangleq \int_1^\infty e^{-xt}x^{-n}dt$ is the n-th order exponential integral.

D. Optimization Problem

The problem of maximizing the sum throughput by the end of the K-th EH interval can be formulated as

$$\max_{p_k,q_k,\tau_k} \quad \sum_{k=1}^{K} R_k \tag{5a}$$

$$\text{s.t.} \quad L\sum_{i=1}^{l} q_i \le \sum_{i=1}^{l} e_i^r,\ \forall l \in [1:K], \tag{5b}$$

$$LT\sum_{i=1}^{l} p_i \le \sum_{i=1}^{l} e_i^t,\ \forall l \in [1:K], \tag{5c}$$

$$\tau_k \in [0,T),\ p_k \ge 0,\ \text{and } q_k \ge 0, \forall k \in [1:K]. \tag{5d}$$

The constraints (5b) and (5c) guarantee the *energy neutrality* of the system, i.e., at each node, energy consumed can not be more than the energy harvested till that time. Also note that τ_k impacts the achievable rate R_k in each EH interval.

Coming up with simple algorithms to solve the optimization problem is desirable in EH networks as the nodes may not have the computational and energy resources for running complex optimization algorithms. However, the ergodic rate expression used in the above optimization problem is not in closed form and offers little insight into the convexity of the problem which is required to reduce the complexity of optimization. This motivates the use of convex bounds on (4) as the objective function in the following optimization problems. Solving these modified problems provides an upper bound on the throughput. Since the constraints in the original and the modified optimization problems are the same, the solution for the modified problem is also feasible in the original problem, and if used in evaluating the exact rate expression in (4), we obtain a lower bound on the throughput. In some settings, we show that the bounds used are very close to the ergodic rate.

Before tackling the above problem, first, we consider a special case in which only the RX harvests energy. Later, the general case with both the TX and the RX harvesting energy is studied.

IV. EH Receiver

In this setting, the RX harvests energy from the environment, whereas the TX is connected to the power grid so that it has a fixed power supply at all times. Therefore, there are no EH constraints at the TX, and constraints (5c) can be ignored. However, there is now a constraint on the average transmission power at each data frame of the k-th EH interval i.e., $p_k \le p, \forall k$. The expected value ν_k is given by [18], [19]

$$\mathrm{E}[\nu_k] = 1 - 2^{b_k}\beta\left(2^{b_k}, \frac{M}{M-1}\right), \tag{6}$$

where $\beta(x,y)$ denotes the beta function. Using the quantization error bound in [19, Lemma 6], (6) can be bounded as[1]

$$\mathrm{E}[\nu_k] \le \nu_k^u \triangleq 1 - \left(\frac{M-1}{M}\right)2^{\frac{-b_k}{M-1}}. \tag{7}$$

Applying Jensen's inequality on (2), substituting (7) and (3), and using the fact that $\mathrm{E}\|\boldsymbol{h}\|^2 = M$, an upper bound on the

[1]This bound is universal in the sense that it applies to any b_k-bit quantization of an isotropically distributed vector, not necessarily limited to RVQ.

ergodic rate $R_k^u \triangleq R^u\left(p_k, q_k, \tau_k\right)$ is obtained as

$$R_k^u = t_k \log_2\left[1 + \frac{p_k M}{t_k}\left(1 - \frac{M-1}{M}\left(1 + \frac{q_k}{\tau_k \sigma^2}\right)^{\frac{-\tau_k}{M-1}}\right)\right], \tag{8}$$

where $t_k \triangleq \left(1 - \frac{\tau_k}{T}\right)$.

We now illustrate the tightness of the upper bound. Applying the Jensen's inequality on (2), $R_k^u - R_k$ can be lower bounded as

$$\begin{aligned} R_k^u - R_k \geq t_k \log_2\left(1 + \frac{p_k}{t_k} M \nu_k^u\right) - \\ t_k \, \mathrm{E}_{||\boldsymbol{h}||^2} \log_2\left(1 + \frac{p_k}{t_k}\left\|\boldsymbol{h}\right\|^2 \mathrm{E}[\nu_k]\right). \end{aligned} \tag{9}$$

Since (2) is a concave function of ν_k and $\nu_k \in [0,1]$, applying Theorem 1 on (2), we have

$$R_k \geq t_k \, \mathrm{E}_{||\boldsymbol{h}||^2} \log_2\left(1 + \frac{p_k}{t_k}\left\|\boldsymbol{h}\right\|^2\right) \mathrm{E}[\nu_k] \tag{10}$$

Now using (10), $R_k^u - R_k$ can be upper bounded as

$$\begin{aligned} R_k^u - R_k \leq t_k \log_2\left(1 + \frac{p_k}{t_k} M \nu_k^u\right) - \\ t_k \, \mathrm{E}_{||\boldsymbol{h}||^2} \log_2\left(1 + \frac{p_k}{t_k}\left\|\boldsymbol{h}\right\|^2\right) \mathrm{E}[\nu_k] \end{aligned} \tag{11}$$

Since both $\lim_{b_k \to \infty} \nu_k^u = 1$ and $\lim_{b_k \to \infty} \mathrm{E}[\nu_k] = 1$ [18], and using (9) and (11), we have,

$$\Delta R_k \triangleq \lim_{b_k \to \infty} R_k^u - R_k = t_k \, \mathrm{E}_{||\boldsymbol{h}||^2} \log_2\left(\frac{t_k + p_k M}{t_k + p_k \left\|\boldsymbol{h}\right\|^2}\right). \tag{12}$$

Further, for all feasible τ_k, in the low power regime,

$$\lim_{p_k \to 0} \Delta R_k = 0, \tag{13}$$

and in the high power regime,

$$\begin{aligned} \lim_{p_k \to \infty} \Delta R_k &= t_k \left(\log_2 M - \mathrm{E}_{||\boldsymbol{h}||^2} \log_2 ||\boldsymbol{h}||^2\right) \\ &\leq \log_2 M - \mathrm{E}_{||\boldsymbol{h}||^2} \log_2 ||\boldsymbol{h}||^2. \end{aligned} \tag{14}$$

From the above analysis, it can be seen that when the RX has enough harvested energy to send large number of feedback bits, in the low power regime the bound is tight, and in the high power regime the difference is bounded by a constant. For example, it is 0.1958 for $M = 4$, and also note that $\lim_{M \to \infty} \log_2 M - \mathrm{E}_{||\boldsymbol{h}||^2} \log_2 ||\boldsymbol{h}||^2 = 0$.

Using (8) as the objective function, the modified optimization problem can be written as follows,

$$\max_{p_k, q_k, \tau_k} \quad \mathcal{U} = \sum_{k=1}^{K} R_k^u \tag{15a}$$

$$\text{s.t.} \quad L \sum_{i=1}^{l} q_i \leq \sum_{i=1}^{l} e_i^r, \forall l \in [1:K], \tag{15b}$$

$$p_k \leq p, \quad \text{and } p_k \geq 0, \ \forall k \in [1:K], \tag{15c}$$

$$\tau_k \in [0, T), \quad \text{and} \quad q_k \geq 0, \quad \forall k \in [1:K], \tag{15d}$$

where p is the power constraint at the transmitter.

As the objective function is monotonic in q_k and p_k, the constraint in (15b) must be satisfied with equality for $l = K$, and the first constraint in (15c) must be satisfied with equality, i.e., $p_k = p, \forall k$; otherwise, we can always increase q_K, p_k, and hence, the objective function, without violating any constraints. Now it remains to optimize over the variables q_k and τ_k.

The feasible set is represented as

$$\mathfrak{F} = \left\{\boldsymbol{q}, \boldsymbol{\tau} | q_k, \tau_k \text{ satisfy (15b), (15d) } \forall k\right\}, \tag{16}$$

where $\boldsymbol{q} = [q_1, \ldots, q_K]$ and $\boldsymbol{\tau} = [\tau_1, \ldots, \tau_K]$. To show that the above problem is a convex optimization problem, we make use of the following lemma.

Lemma 1: If the function $f\left(x,t\right) : \mathbb{R}_+^2 \to \mathbb{R}_+$ is concave, and $g\left(y,z\right) : \mathbb{R}_+^2 \to \mathbb{R}_+$ is concave and monotonically increasing in each argument, then the function $h\left(x,y,t\right) = \left(1 - \frac{t}{T}\right) g\left(\frac{y}{1-\frac{t}{T}}, \frac{f(x,t)}{1-\frac{t}{T}}\right)$ is concave $\forall \left(x,y\right) \in \mathbb{R}_+^2, t \in [0,T)$.

Proof: The proof is similar to that of showing the perspective of a concave function is concave. See Appendix. ■

Proposition 1: The objective function of the optimization problem (15) is concave.

Proof: See Appendix. ■

Since the objective function in (15) is concave and the constraints are linear, it has a unique maximizer [20]. Using the concavity of the objective function, we show that the optimal energy allocation vector is the most majorized feasible energy vector.

Proposition 2: The global optimum of (15) is obtained at $\left(\boldsymbol{q}^*, \boldsymbol{\tau}^*\right)$, where $\boldsymbol{q}^* \preceq \boldsymbol{q}, \forall \left(\boldsymbol{q}, \boldsymbol{\tau}\right) \in \mathfrak{F}$, and τ_k^* is the solution of the following equation

$$\frac{\partial R_k^u}{\partial \tau_k}|_{\left(q_k^*, \tau_k^*\right)} = 0, \ \forall k \in [1:K]. \tag{17}$$

Proof: Consider the following equivalent form of (15), where the optimization is performed in two steps.

$$\max_{\boldsymbol{q}} \ \tilde{\mathcal{U}}\left(\boldsymbol{q}\right) \ \text{ s.t. } \forall \left(\boldsymbol{q}, \boldsymbol{\tau}\right) \in \mathfrak{F}, \tag{18}$$

where $\tilde{\mathcal{U}}\left(\boldsymbol{q}\right)$ is obtained by

$$\tilde{\mathcal{U}}\left(\boldsymbol{q}\right) = \max_{\boldsymbol{\tau}} \ \mathcal{U}\left(\boldsymbol{q}, \boldsymbol{\tau}\right) \ \text{ s.t. } \forall \left(\boldsymbol{q}, \boldsymbol{\tau}\right) \in \mathfrak{F}. \tag{19}$$

Since $\mathcal{U}$ is a concave function over the convex set $\mathfrak{F}$, the function $\tilde{\mathcal{U}}\left(\boldsymbol{q}\right)$ is concave, where the domain of $\tilde{\mathcal{U}}$ is the set $\tilde{\mathfrak{F}} = \left\{\boldsymbol{q} | \left(\boldsymbol{q}, \boldsymbol{\tau}\right) \in \mathfrak{F}\right\}$ [20, 3.2.5]. $\mathcal{U} = \sum_{k=1}^{K} R_k^u$ is continuous, differentiable and concave in $\tau_k \in [0, T)$. Furthermore, for given q_k, R_k^u approaches $\log_2\left(1+p\right)$ and 0, as τ_k approaches 0 and T, respectively. Therefore, the unique maximizer of (19) lies in $[0, T)$, and it is obtained at

$$\frac{\partial \mathcal{U}}{\partial \tau_k}|_{\tau_k^*} = \frac{\partial R_k^u}{\partial \tau_k}|_{\tau_k^*} = 0, \ \forall k \in [1:K]. \tag{20}$$

From above, as τ_k^* is only a function of q_k,

$$\tilde{\mathcal{U}}\left(\boldsymbol{q}\right) = \sum_{k=1}^{K} \tilde{R}_k^u \tag{21}$$

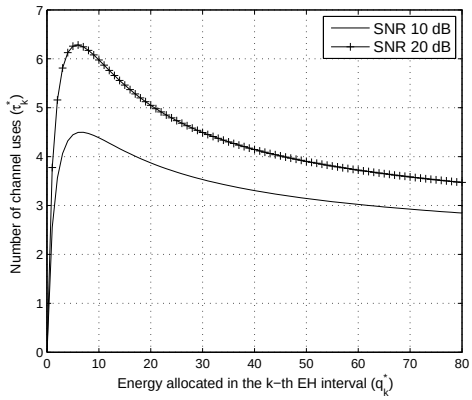

Figure 3. Optimal number of channel uses for sending feedback.

where $\tilde{R}_k^u \triangleq \tilde{R}^u(q_k) = R^u(q_k, \tau_k^*(q_k))$. Using (21) and Theorem 2, $\tilde{\mathcal{U}}(\boldsymbol{q}^*) \geq \tilde{\mathcal{U}}(\boldsymbol{q}), \forall \boldsymbol{q} \in \tilde{\mathfrak{F}}$. Finding the optimal energy allocation vector $\boldsymbol{q}^*$ under the EH constraints turns out be a well known problem, and the algorithm to construct $\boldsymbol{q}^*$ is given in various works [21]–[23]. The proof that the algorithm constructs the most majorized feasible energy vector is given in [23]. Since the optimal energy allocation vector is $\boldsymbol{q}^*$, the optimal $\boldsymbol{\tau}^*$ is obtained by (17). ■

A brief description of the algorithm tailored to this work is given next, while the details can be found in [21]–[23]. There is no closed form expression for the solution of (17), hence we resort to numerical methods to obtain $\boldsymbol{\tau}^*$. Fig. 3 shows the behavior of τ_k^* as a function of the allocated energy q_k^*.

A. Optimal Energy Allocation

From Definition 1, we can see that the components of the most majorized energy vector are "less spread out" than any other feasible energy vector. Therefore, the algorithm essentially tries to make the energy vector as equalized as possible. This is done by spreading the energy to future intervals. However, note that the energy arriving in later intervals cannot be spread to earlier intervals due to the EH constraints. The Optimal Energy Allocation (OEA) algorithm, given in Algorithm 1, divides the EH intervals into $|\mathcal{S}|$ energy bands whose indices form the set $\mathcal{S} = \{B_0, B_1, \dots B_{|\mathcal{S}|}\}$, where $B_i < B_j, \forall i < j$, $B_0 = 0$, and $B_{|\mathcal{S}|} = K$. The i-th energy band contains the EH intervals with indices $k \in [B_{i-1}+1 : B_i]$. Moreover, the optimal allocated energy values in each EH interval belonging to the i-th energy band are equal, and denoted by $q_{(i)}^*$. The energy vector $\boldsymbol{q}^*$ obtained by $[\boldsymbol{q}^*, \mathcal{S}_r] = \text{OEA}(K, \{e_i^r/L\})$, has the following properties:

(P1) $q_k^* = q_{(i)}^* = \frac{\sum_{l=B_{i-1}+1}^{t_i} e_l^r}{L(B_i - B_{i-1})}$, $\forall k \in [B_{i-1}+1 : B_i]$.

(P2) The entries $q_{(i)}^*$ are strictly monotonic, i.e., $q_{(1)}^* < q_{(2)}^* < \dots < q_{(|\mathcal{S}|)}^*$.

Input : EH intervals K; Harvested energy $\{e_i\}$
Output: Energy allocation $\boldsymbol{o}^\star$, Energy band indices $\mathcal{S} = \{B_0, B_1, \dots B_{|\mathcal{S}|}\}$

```
// initialization
B_0 := 0;
for i = 1 : K do
    for k = K : −1 : (t_{i−1} + 1) do
        (i) o_l^⋆ = (Σ_{j=B_{i−1}+1}^{k} e_j) / (k − B_{i−1}),  l ∈ {B_{i−1} + 1, ..., k}
        if Σ_{i=1}^{l} o_i^⋆ ≤ Σ_{i=1}^{l} e_i, l = 1, ..., K then
            B_i = k;
            Save {o_1^⋆, ··· , o_k^⋆}
            break;
        end
    end
    if B_i == K then
        break;
    end
end
```

Algorithm 1: Optimal Energy Allocation (OEA) algorithm

V. EH Transmitter and Receiver

In this section, we consider the general case where both the TX and the RX harvest energy. Note that if the TX is silent in the k-th interval, i.e., $p_k = 0$, there is no incentive for the RX to send feedback in this interval. Therefore, without loss of optimality we only consider EH profiles where $e_1^t > 0$. Otherwise, if there is an EH profile such that $e_k^t = 0, k \in [1 : m-1]$, then $p_k = 0, k \in [1 : m-1]$ due to the constraints in (5c). In these intervals the RX simply accumulates the harvested energy, and without loss of optimality we can have a new EH profile with $\tilde{e}_1^t = e_{i+m-1}^t, \forall i \in [1 : K-m+1]$, and $\tilde{e}_1^r = \sum_{k=1}^m e_k^r$ and $\tilde{e}_i^r = e_{i+m-1}^r, \forall i \in [2 : K-m+1]$ for further analysis.

The ergodic rate upper bound in (8) is not concave, but concave in each variable given the other variables are fixed. To obtain a simple algorithm and an upper bound on the throughput, we follow a similar approach as in the previous section, and use a concave upper bound on (8) as the objective function for throughput optimization.

This bound is obtained by using a hypothetical system in which the transmission power is 1 watt higher than the actual transmission power of the system, which is p_k/t_k. Plugging this into the upper bound in (8), a new upper bound $R_k^{ub} \triangleq R^{ub}(p_k, q_k, \tau_k)$ on the ergodic rate is obtained:

$$R_k^{ub} = t_k \log_2 \left(1 + \left(1 + \frac{p_k}{t_k}\right) \frac{f_k}{t_k}\right), \tag{22}$$

where $t_k \triangleq 1 - \frac{\tau_k}{T}$ and $f_k \triangleq M - (M-1)\left(1 + \frac{q_k}{\tau_k \sigma^2}\right)^{\frac{-\tau_k}{M-1}}$. We now illustrate the tightness of the upper bound in (22) in the low and high power regimes. For all feasible τ_k, p_k and q_k, we can see that $0 < t_k \leq 1$ and $1 \leq f_k \leq M$. Consider

$$R_k^{ub} - R_k^u = t_k \log_2 \left(\frac{t_k^2 + t_k f_k + p_k f_k}{t_k + p_k f_k}\right) - t_k \log_2 (t_k) \tag{23}$$

Note that (23) is decreasing in p_k for fixed τ_k and q_k. Since τ_k, f_k are bounded, for fixed τ_k and q_k, in the low power

regime

$$\lim_{p_k\to 0} R_k^{ub} - R_k^u = t_k \log_2\left(1+\frac{f_k}{t_k}\right) \leq \log_2\left(1+M\right), \tag{24}$$

and in the high power regime,

$$\lim_{p_k\to \infty} R_k^{ub} - R_k^u = -t_k \log_2(t_k) \leq 0.5. \tag{25}$$

From the above analysis, it can be seen that, (23) decreases as the power is increased, and it is bounded by a constant in the high power regime. By using (22), the modified throughput maximization problem is formulated as

$$\max_{p_k,q_k,\tau_k} \quad \mathcal{U}_1 = \sum_{k=1}^{K} R_k^{ub} \tag{26a}$$

$$\text{s.t.} \quad L\sum_{i=1}^{l} q_i \leq \sum_{i=1}^{l} e_i^r, \forall l \in [1:K], \tag{26b}$$

$$LT\sum_{i=1}^{l} p_i \leq \sum_{i=1}^{l} e_i^t, \forall l \in [1:K], \tag{26c}$$

$$\tau_k \in [0,T),\ p_k \geq 0,\ q_k \geq 0,\ \text{and } \forall k \in [1:K]. \tag{26d}$$

Since the objective function is monotonic in q_k and p_k, the constraints in (26b) and (26c) must be satisfied with equality for $l = K$, otherwise, we can always increase q_K, p_K, and hence the objective function, without violating any constraints. The feasible set is represented as

$$\mathfrak{J} = \left\{(\boldsymbol{p},\boldsymbol{q},\boldsymbol{\tau})\,|p_k,q_k,\tau_k \text{ satisfy (26b), (26c) and (26d) } \forall k\right\},$$

where $\boldsymbol{p} = [p_1,\ldots,p_K]$, $\boldsymbol{q} = [q_1,\ldots,q_K]$ and $\boldsymbol{\tau} = [\tau_1,\ldots,\tau_K]$.

Proposition 3: The objective function in the optimization problem (26) is concave.

Proof: See Appendix. ∎

Since the objective function in (26) is concave and the constraints are linear, it has a unique maximizer [20]. Consider the following equivalent form of (26), where the optimization is performed in two steps.

$$\max_{\boldsymbol{p},\boldsymbol{q}} \tilde{\mathcal{U}}_1(\boldsymbol{p},\boldsymbol{q}) \ \text{ s.t. } \forall(\boldsymbol{p},\boldsymbol{q},\boldsymbol{\tau}) \in \mathfrak{J}, \tag{27}$$

where $\tilde{\mathcal{U}}_1(\boldsymbol{p},\boldsymbol{q})$ is obtained by

$$\tilde{\mathcal{U}}_1(\boldsymbol{p},\boldsymbol{q}) = \max_{\boldsymbol{\tau}} \mathcal{U}_1(\boldsymbol{p},\boldsymbol{q},\boldsymbol{\tau}) \ \text{ s.t. } \forall(\boldsymbol{p},\boldsymbol{q},\boldsymbol{\tau}) \in \mathfrak{J}. \tag{28}$$

Since $\mathcal{U}_1$ is a concave function over the convex set $\mathfrak{J}$, the function $\tilde{\mathcal{U}}_1$ is concave with domain $\tilde{\mathfrak{J}} = \{(\boldsymbol{p},\boldsymbol{q})\,|\,(\boldsymbol{p},\boldsymbol{q},\boldsymbol{\tau}) \in \mathfrak{J}\}$ [20, 3.2.5]. $\mathcal{U}_1 = \sum_{k=1}^{K} R_k^{ub}$ is continuous, differentiable and concave in $\tau_k \in [0,T)$. Furthermore, for given p_k and q_k, R_k^{ub} approaches $\log_2(2+p_k)$ and 0, as τ_k approaches 0 and T, respectively. Therefore, the unique maximizer of (28), $\tau_k^*, \forall k$ lies in $[0,T)$, and it is obtained as

$$\frac{\partial \mathcal{U}_1}{\partial \tau_k}|_{\tau_k^*} = \frac{\partial R_k^{ub}}{\partial \tau_k}|_{\tau_k^*} = 0,\ \forall k \in [1:K]. \tag{29}$$

As τ_k^* is only a function of q_k and p_k, (27) can be written as

$$\max_{p_k,q_k} \quad \tilde{\mathcal{U}}_1 = \sum_{k=1}^{K} \tilde{R}_k^{ub} \ \text{ s.t. } \forall k, (p_k,q_k) \in \tilde{\mathfrak{J}}, \tag{30}$$

where $\tilde{R}_k^{ub} \triangleq \tilde{R}^{ub}(p_k,q_k) = R^{ub}(p_k,q_k,\tau_k^*(p_k,q_k))$.

In order to get an insight on how the optimal solution of (27) may look like, consider a simple scenario in which there is only a sum power constraint at the TX and the RX, i.e., the constraints in (26b), (26c) has to be satisfied for only $l = K$. In this case, by Jensen's inequality, the uniform power allocation at the TX and the RX is optimal[2]. However, due to the EH constraints, this may not be feasible. Using this intuition, we can see that the optimal policy tries to equalize the powers as much as possible, while satisfying the EH constraints. Next, we consider the case in which the EH profiles at the TX and the RX are similar, and show that the optimization problem is considerably simplified.

A. Similar EH Profiles

The EH profiles are similar in the sense that the most majorized feasible vectors obtained from the EH profiles of the TX and RX, $\boldsymbol{p}^*$ and $\boldsymbol{q}^*$, have the same structure, i.e., if $p_i^* = c_1, \forall i \in [m:n]$, then $q_i^* = c_2, \forall i \in [m:n]$ for some constants $c_1, c_2 \geq 0$. We now give a formal definition.

Definition 4: By using the OEA algorithm, let $[\boldsymbol{q}^*, \mathcal{S}_r] = \text{OEA}(K, \{e_i^r/L\})$ and $[\boldsymbol{p}^*, \mathcal{S}_t] = \text{OEA}(K, \{e_i^t/LT\})$. EH profiles at the TX and the RX are said to be *similar* if $\mathcal{S}_r = \mathcal{S}_t$.

From Section II, we can see that the definition of majorization for the vector case does not directly extend to the matrix case. If OEA algorithm is used at the TX and RX separately, we get the most individually majorized power vectors, which in general may not be the optimal solution of (27). However, we now show that if the EH profiles are similar, the above mentioned approach is indeed optimal.

Proposition 4: If the EH profiles at the TX and the RX are similar then $(\boldsymbol{q}^*, \boldsymbol{p}^*, \boldsymbol{\tau}^*)$ is the global optimum of (26), where $\boldsymbol{q}^* \preceq \boldsymbol{q}, \boldsymbol{p}^* \preceq \boldsymbol{p},\ \forall(\boldsymbol{q},\boldsymbol{p},\boldsymbol{\tau}) \in \mathfrak{J}$, and τ_k^* is the solution of

$$\frac{\partial R_k^{ub}}{\partial \tau_k}|_{(p_k^*,q_k^*,\tau_k^*)} = 0,\ \forall k \in [1:K]. \tag{31}$$

Proof: See Appendix. ∎

B. Different EH Profiles

Unfortunately, we could not find a simple algorithm to solve (26) in a general setting where the EH profiles are not similar. In (30), if one variable is fixed, optimizing over the other variable has a *directional* or *staircase water-filling* interpretation [4], [21], however, the difficulty lies in the fact that there is no closed form expression for $\tilde{R}_k^{ub}$. Nonetheless, based on the convexity of the objective function, some properties of the optimal solution are given below.

Lemma 2: Under the optimal policy, the transmission power p_k, and the energy used to send the feedback q_k are non-decreasing in $k, \forall k \in [1:K]$.

Lemma 3: Under the optimal policy, at the time instants at which R^{ub} changes, the energy buffer of either the TX or the RX is emptied.

The proofs of the above lemmas are given in Appendix.

[2]In this section, with slight abuse of terminology we use the terms RX power and RX energy interchangeably.

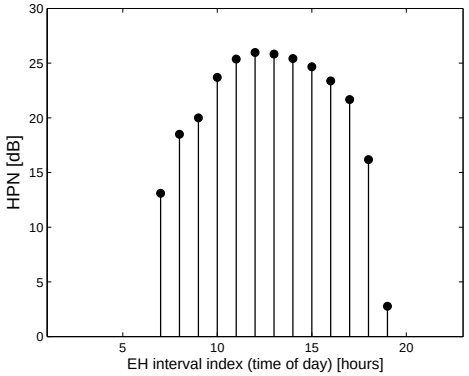

Figure 4. Model for a solar energy harvesting profile.

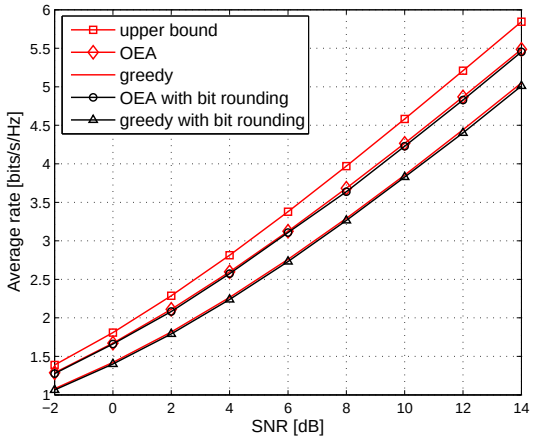

Figure 5. Ergodic rate with only an EH RX, and $M = 4$.

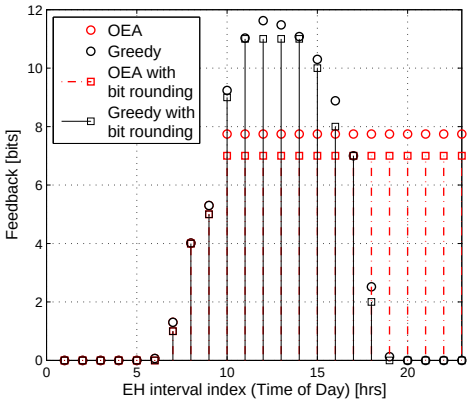

Figure 6. Feedback load at downlink SNR of 10 dB, $M = 4$.

VI. Numerical Results

We start by considering the case in which the RX harvests energy, while the TX has a constant power supply. We assume that the RX is equipped with a solar EH device. Following [24], solar irradiance data is taken from the database reported in [25]. Each EH interval is of duration $\Delta = 1$ hour, $T = 200$ ms, resulting in $L = 18000$ frames. The harvested power from the irradiance data can be calculated as, $p_{harv} = I[\text{Watt}/m^2] \times Area[m^2] \times \rho$, where ρ is the efficiency of the harvester. A hypothetical solar panel of variable area is assumed. The area of the panel is adjusted such that we have the EH profile shown in Fig. 4 at the RX. In Fig. 4, the harvested power to noise ratio (HPN) in each EH interval $\frac{e_k^r}{\Delta\sigma^2}$ is shown.

Using this EH profile, throughput of different feedback policies is shown in Fig. 5. In Fig. 5, OEA represents the proposed policy in which the energy vector is obtained by using the OEA algorithm, and then the optimal time span of feedback τ_k^* is obtained by solving (20). In the greedy scheme, the consumed energy is equal to the harvested energy in that interval, i.e., $q_k = e_k^r/L$, and then optimization is performed only over τ_k, given q_k. The performance of the above policies when the feedback bits are rounded to the largest previous integer is also shown. We can see that the proposed approach outperforms the greedy policy by 1.6 dB at a rate of 4 bits/s/Hz. Also the rate loss due to bit rounding is negligible. In Fig. 6, feedback bit allocation is shown for the above mentioned policies for a downlink SNR of 10 dB. From Fig. 6, we can see that with the proposed strategy, feedback bit allocation is equalized as much as possible.

We now consider the case in which both the TX and the RX harvest energy, with similar EH profiles. The same EH profile in Fig. 4 is separately used at both the RX and the TX, hence the EH profiles are similar. In Fig. 7, the throughput of different schemes is shown at various mean HPN values at the TX. The mean HPN at the TX is varied by increasing the harvester area at the TX, i.e., the EH profile is multiplied by a positive number (area), while keeping the same shape and efficiency. In Fig. 7, OEA represents the proposed policy in which the energy vector at the TX and the RX is obtained by using the OEA algorithm, and then the optimal time span of feedback τ_k^* is obtained by solving (29). In the greedy scheme, the allocated energy is equal to the harvested energy in that interval, i.e., at the TX $p_k = e_k^t/LT$, at the RX $q_k = e_k^r/L$, and then optimization is performed only over τ_k, given p_k and q_k. The difference in throughput between the greedy and OEA is small when the average HPN is low, and it increases with the HPN. In contrast to the OEA scheme, using the greedy approach with the solar EH profile results in some EH intervals being allocated zero energy, and therefore does not scale by increasing the harvester area. This particularly hurts the greedy policy's throughput in the high HPN regime as the multiplexing gain (pre-log factor) is reduced.

Finally, we consider a case with non-similar EH profiles, where the EH profiles are generated independently at the TX and the RX, and they are i.i.d. with exponential distribution. EH profiles are verified not to be similar according to Definition 4. Similarly to Fig. 7, in Fig. 8, the mean HPN at the TX is varied by multiplying the EH profile by a constant, while keeping the same shape. Since we could not find a simple algorithm in this case, CVX solver is used to solve the optimization problem [20], and is denoted as CVX in Fig. 8. As we can see, the heuristic of using the OEA approach performs quite well even in the non-similar EH profile scenario. The energy allocation at the TX and the

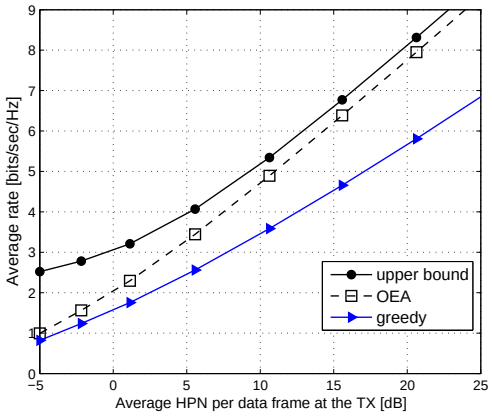

Figure 7. Ergodic rate for similar EH profiles, $M = 4$.

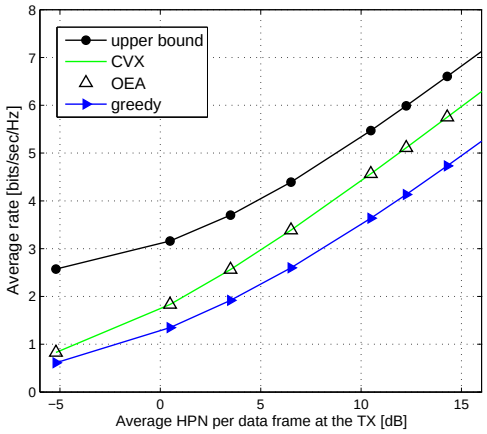

Figure 8. Ergodic rate for non-similar EH profiles, $M = 4$.

RX are shown in Fig. 9 for the above mentioned policies at an average per frame HPN of 0.5 dB at the TX. Different from Fig. 7, in Fig. 8 the rate scaling with average HPNs is same for both the greedy and the OEA policies. For the greedy policy, the allocated energy in an EH interval scales with the increasing mean HPN, in contrast to the solar EH profile, for which the allocated energy is zero in some intervals.

VII. Conclusion

In contrast to the existing literature on the design of energy harvesting communication systems, we have assumed in this paper that the perfect channel state information is available only at the receiver side; and we have studied the problem of CSI feedback design in a p2p MISO channel under EH constraints at both the TX and the RX. Since the exact expressions of throughput are complicated, concave upper bounds have been used in the optimization problems. We have first considered the case in which only the RX harvests energy, and optimized the feedback policy under EH constraints. Later, the general case, in which both the TX and the RX harvest energy, is analyzed. We have shown that, if EH profiles are similar, the optimization problem can be considerably simplified. We

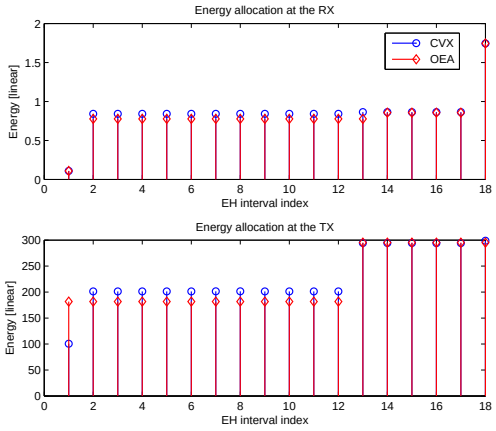

Figure 9. Energy allocation at the TX and the RX, $M = 4$.

remark that the result obtained in Proposition 4 is general, and, for example, it can be used in a network setting in which a concave utility is to be maximized in the presence of EH nodes with similar harvesting profiles and infinite size energy buffers. Numerical results show that the proposed policies not only outperform the greedy policy, but also achieve performances very close to the theoretical upper bound. Our work sheds light on the design of feedback-enabled multi-antenna systems when the nodes depend on EH devices for their energy.

Appendix

A. Proof of Lemma 1

Let $X_1 = [x_1\ y_1\ t_1]^{\mathrm{T}}, X_2 = [x_2\ y_2\ t_2]^{\mathrm{T}}$, we have

$$\begin{aligned} & h\left(\lambda X_1 + (1-\lambda) X_2\right) \\ & = \Theta g\left(\frac{\lambda y_1 + (1-\lambda) y_2}{\Theta}, \frac{f\left(\overline{x}, \overline{t}\right)}{\Theta}\right) \\ & \overset{(a)}{\geq} \Theta g\left(\frac{\lambda y_1 + (1-\lambda) y_2}{\Theta}, \frac{\lambda f_1 + (1-\lambda) f_2}{\Theta}\right) \\ & = \Theta g\left(\frac{\Theta_1 y_1}{\Theta \alpha_1} + \frac{\Theta_2 y_2}{\Theta \alpha_2}, \frac{\Theta_1 f_1}{\Theta \alpha_1} + \frac{\Theta_2 f_2}{\Theta \alpha_2}\right) \\ & \overset{(b)}{\geq} \Theta_1 g\left(\frac{y_1}{\alpha_1}, \frac{f_1}{\alpha_1}\right) + \Theta_2 g\left(\frac{y_2}{\alpha_2}, \frac{f_2}{\alpha_2}\right) \\ & = \lambda h\left(X_1\right) + (1-\lambda) h\left(X_2\right), \end{aligned} \tag{32}$$

where $\overline{x} \triangleq \lambda x_1 + (1-\lambda) x_2$, $\overline{t} \triangleq \lambda t_1 + (1-\lambda) t_2$, $f_1 \triangleq f\left(x_1, t_1\right)$, $f_2 \triangleq f\left(x_2, t_2\right)$, $\Theta_1 \triangleq \lambda\left(1 - \frac{t_1}{T}\right)$ and $\Theta_2 \triangleq (1-\lambda)\left(1 - \frac{t_2}{T}\right), \Theta = \Theta_1 + \Theta_2$, $\alpha_1 \triangleq \left(1 - \frac{t_1}{T}\right)$, $\alpha_2 \triangleq \left(1 - \frac{t_2}{T}\right)$. Here

(a) follows from the fact that $f\left(x, t\right)$ is concave, and $g\left(y, z\right)$ is monotonically increasing in each argument,

(b) follows from the fact that $\frac{\Theta_1}{\Theta} + \frac{\Theta_2}{\Theta} = 1$, and $g\left(y, z\right)$ is concave.

B. Proof of Proposition 1

Reproducing the ergodic rate bound in (8) with $p_k = P, \forall k$, we have

$$R^u\left(q_k, \tau_k\right) = t_k \log_2\left(1 + \frac{P f_k}{t_k}\right), \tag{33}$$

where $t_k \triangleq 1-\frac{\tau_k}{T}, f_k \triangleq (M-M-1(1+\frac{q_k}{\tau_k\sigma^2})^{\frac{-\tau_k}{M-1}})$. Since b_k in (3) is concave in q_k and τ_k, it can be easily seen that $2^{-\frac{b_k}{M-1}} = \left(1+\frac{q_k}{\tau_k\sigma^2}\right)^{\frac{-\tau_k}{M-1}}$ is convex, and hence, f_k is concave. Using Lemma 1 with $g(y,z)=\log_2(1+z)$ and f_k, we can see that R_k^u is concave. Since the objective function in (15) is the summation of R_k^u's, it is also concave.

C. Proof of Proposition 3

First, we show that $g(y,z)=\log_2(1+(1+y)z), (y,z)\in\mathbb{R}_+^2$ is concave for $y\geq 0, z\geq 1$. The Hessian of g is given by

$$\mathbf{J}=\frac{1}{\beta}\begin{pmatrix}-z^2 & 1\\ 1 & -(1+y)^2\end{pmatrix}, \tag{34}$$

where $\beta=\log_e 2\,(1+(1+y)z)^2>0$. Consider $\boldsymbol{u}^{\mathrm{T}}\mathbf{J}\boldsymbol{u} = -\frac{1}{\beta}\left(a^2z^2+b^2(1+y)^2-2ab\right)$, where $\boldsymbol{u}=[a\ b]^{\mathrm{T}}\in\mathbb{R}^2$. It can be easily seen that $\boldsymbol{u}^{\mathrm{T}}\mathbf{J}\boldsymbol{u}\leq 0$ for $ab\leq 0$. For $ab>0$, since $z(1+y)\geq 1$, $\boldsymbol{u}^{\mathrm{T}}\mathbf{J}\boldsymbol{u} = -\frac{1}{\beta}\left[(az-b(1+y))^2+2ab(z(1+y)-1)\right]\leq 0$. As Hessian is negative semidefinite, $g(y,z)$ is concave. Reproducing the ergodic rate bound in (22), we have

$$R_k^{ub}=t_k\log_2\left(1+\left(1+\frac{p_k}{t_k}\right)\frac{f_k}{t_k}\right), \tag{35}$$

where t_k and f_k are as defined before.

By following the similar steps in Proposition 1, f_k can be shown to be concave. Using Lemma 1 with $g(y,z)$ and f_k, we can see that R_k^{ub} is concave. Since the objective function in (26) is the summation of R_k^{ub}'s, it is also concave.

D. Proof of Proposition 4

First, $(\boldsymbol{p}^*,\boldsymbol{q}^*)$ is shown to be the solution of (30) and then $\boldsymbol{\tau}^*$ is obtained by (31). Before solving (30), we prove that

$$\begin{aligned}(\boldsymbol{p}^*,\boldsymbol{q}^*)=&\arg\max_{g,p_k,q_k}\ \sum_{k=1}^{K} g(p_k,q_k)\\ &\text{s.t. } \forall k,(p_k,q_k)\in\tilde{\mathfrak{J}}, g\in\mathfrak{C},\end{aligned} \tag{36}$$

where $\mathfrak{C}$ is the set of all continuous concave functions. As (30) is a special case of (36), $(\boldsymbol{p}^*,\boldsymbol{q}^*)$ is also the solution of (30).

Before starting, we note that the notations and properties of the OEA algorithm discussed in Section IV-A are used throughout the proof. By contradiction, let us assume that there exists a $[\hat{\boldsymbol{p}}^{\mathrm{T}}\ \hat{\boldsymbol{q}}^{\mathrm{T}}]^{\mathrm{T}}\neq[\boldsymbol{p}^{*\mathrm{T}}\ \boldsymbol{q}^{*\mathrm{T}}]^{\mathrm{T}}$ and $(\hat{\boldsymbol{p}},\hat{\boldsymbol{q}})$ be the solution of (36). Then, by Theorem 3 we have,

$$[\hat{\boldsymbol{p}}^{\mathrm{T}}\ \hat{\boldsymbol{q}}^{\mathrm{T}}]^{\mathrm{T}}\preceq[\boldsymbol{p}^{\mathrm{T}}\ \boldsymbol{q}^{\mathrm{T}}]^{\mathrm{T}},\ \forall(\boldsymbol{p},\boldsymbol{q})\in\tilde{\mathfrak{J}}. \tag{37}$$

Since $(\boldsymbol{p}^*,\boldsymbol{q}^*)\in\tilde{\mathfrak{J}}$, by (37) and Definition 3,

$$[\hat{\boldsymbol{p}}^{\mathrm{T}}\ \hat{\boldsymbol{q}}^{\mathrm{T}}]^{\mathrm{T}}=\left[\boldsymbol{p}^{*\mathrm{T}}\ \boldsymbol{q}^{*\mathrm{T}}\right]^{\mathrm{T}}\mathbf{D}. \tag{38}$$

By the feasibility constraint in (26b),

$$\sum_{j=B_{i-1}+1}^{B_i}\hat{q}_j\leq V_i=\sum_{j=B_{i-1}+1}^{B_i}e_j^r/L, \tag{39}$$

where B_i's are the energy band indices as explained in Section IV-A.

Applying (39) for $i=1$, and remembering that $B_0=0$, we get

$$\sum_{j=1}^{B_1}\hat{q}_j=\sum_{j=1}^{B_1}\sum_{i=1}^{K}q_i^*d_{i,j}\leq V_1. \tag{40}$$

By (P1) and (P2) in Section IV-A, $q_i^*=q_{(1)}^*+L_i$, where

$$\begin{aligned}&L_i=0\ \ \forall i\in[1:B_1],\\ &L_i>0\ \ \forall i\in[B_1+1:K].\end{aligned} \tag{41}$$

From (40) and (41)

$$\sum_{j=1}^{B_1}\sum_{i=1}^{K}q_{(1)}^*d_{i,j}+\sum_{j=1}^{B_1}\sum_{i=B_1+1}^{K}L_id_{i,j}\leq V_1. \tag{42}$$

Using the fact that $\mathbf{D}$ is doubly stochastic and by (P1), $B_1q_{(1)}^*=V_1$, and we have

$$\sum_{j=1}^{B_1}\sum_{i=B_1+1}^{K}L_id_{i,j}\leq 0. \tag{43}$$

From (41) and (43), we get

$$d_{i,j}=0,\ \ \forall i\in[B_1+1:K],\ \forall j\in[1:B_1]. \tag{44}$$

As $\mathbf{D}$ is doubly stochastic, using (P1) and (44),

$$\hat{q}_j=\sum_{i=1}^{B_1}q_{(1)}^*\sum_{i=1}^{B_1}d_{i,j}=q_{(1)}^*=q_j^*,\forall j\in[1:B_1]. \tag{45}$$

Since $\mathbf{D}$ is doubly stochastic, using (44), we get

$$\sum_{i=1}^{B_1}\sum_{j=1}^{K}d_{i,j}=B_1,\quad\sum_{i=1}^{B_1}d_{i,j}=1,\ \forall j\in[1:B_1]. \tag{46}$$

We can rewrite (46) as

$$\sum_{i=1}^{B_1}\sum_{j=1}^{K}d_{i,j}=\sum_{i=1}^{B_1}\sum_{j=1}^{B_1}d_{i,j}+\sum_{i=1}^{B_1}\sum_{j=B_1+1}^{K}d_{i,j}, \tag{47}$$

from which it follows that

$$\sum_{i=1}^{B_1}\sum_{j=B_1+1}^{K}d_{i,j}=0, \tag{48}$$

and hence,

$$d_{i,j}=0,\ \ \forall i\in[1:B_1],\forall j\in[B_1+1:K]. \tag{49}$$

Then applying (39) for $i=2$,

$$\sum_{j=B_1+1}^{B_2}\hat{q}_j=\sum_{j=B_1+1}^{B_2}\sum_{i=1}^{K}q_i^*d_{i,j}\leq V_2. \tag{50}$$

By (P1) and (P2), we have $q_i^*=q_{(2)}^*+L_i$, where

$$\begin{aligned}&L_i<0\ \ \forall i\in[1:B_1],\\ &L_i=0\ \ \forall i\in[B_1+1:B_2],\\ &L_i>0\ \ \forall i\in[B_2+1:K].\end{aligned} \tag{51}$$

From (50) and (51),

$$\sum_{j=B_1+1}^{B_2}\sum_{i=1}^{K} L_i d_{i,j} + \sum_{j=B_1+1}^{B_2}\sum_{i=1}^{K} q^*_{(2)} d_{i,j} \leq V_2. \tag{52}$$

Since $\mathbf{D}$ is doubly stochastic, by (P1), we obtain $(B_2 - B_1)\, q^*_{(2)} = V_2$, and using (49) and (51) in (52), we get

$$\sum_{j=B_1+1}^{B_2}\sum_{i=B_2+1}^{K} L_i d_{i,j} \leq 0, L_i > 0. \tag{53}$$

From (51) and (53) it can be concluded that

$$d_{i,j} = 0, \quad \forall i \in [B_2+1 : K]\,,\ \forall j \in [B_1+1 : B_2]\,. \tag{54}$$

As $\mathbf{D}$ is doubly stochastic, using (P1) together with (49) and (54), we have

$$\hat{q}_j = q^*_{(2)} \sum_{i=B_1+1}^{B_2} d_{i,j} = q^*_{(2)} = q^*_j, \forall j \in [B_1+1 : B_2]\,. \tag{55}$$

Again, since $\mathbf{D}$ is doubly stochastic, using (49) and (54),

$$\begin{aligned} \sum_{i=B_1+1}^{B_2}\sum_{j=1}^{K} d_{i,j} &= B_2 - B_1, \\ \sum_{i=B_1+1}^{B_2} d_{i,j} &= 1,\ \forall j \in [B_1+1 : B_2]\,. \end{aligned} \tag{56}$$

We can rewrite (56) as

$$\sum_{i=B_1+1}^{B_2}\sum_{j=1}^{K} d_{i,j} = \sum_{i=B_1+1}^{B_2}\sum_{j=B_1+1}^{B_2} d_{i,j} + \sum_{i=B_1+1}^{B_2}\sum_{j=B_2+1}^{K} d_{i,j}. \tag{57}$$

From (57) we can see that

$$\sum_{i=B_1+1}^{B_2}\sum_{j=B_2+1}^{K} d_{i,j} = 0, \tag{58}$$

and hence,

$$d_{i,j} = 0, \forall i \in [B_1+1 : B_2] \text{ and } \forall j \in [B_2+1 : K]\,. \tag{59}$$

Continuing this approach for $i = 3, ..., (|\mathcal{S}| - 1)$, we get $\hat{\boldsymbol{q}} = \boldsymbol{q}^*$. Since the EH profiles are similar, replacing $\hat{\boldsymbol{q}}$ by $\hat{\boldsymbol{p}}$ and e^r_j by e^t_j/T in the above proof, we reach the similar conclusion for $\hat{\boldsymbol{p}}$, i.e., $\hat{\boldsymbol{p}} = \boldsymbol{p}^*$. Therefore, $\left[\hat{\boldsymbol{p}}^{\mathrm{T}}\ \hat{\boldsymbol{q}}^{\mathrm{T}}\right]^{\mathrm{T}} = \left[\boldsymbol{p}^{*\mathrm{T}}\ \boldsymbol{q}^{*\mathrm{T}}\right]^{\mathrm{T}}$.

E. Proof of Lemma 2

Assume that at least one of the p_k, q_k is not monotonically increasing in k. Without loss of generality (w.l.o.s) we consider the cases in which $p_k > p_{k+1}, q_k \geq q_{k+1}$ and $p_k < p_{k+1}, q_k > q_{k+1}$. In the case of $p_k > p_{k+1}, q_k \geq q_{k+1}$, we can construct a new feasible policy,

$$\begin{aligned} \tilde{p}_k = \tilde{p}_{k+1} &= \frac{p_k + p_{k+1}}{2}, \\ \tilde{q}_k = \tilde{q}_{k+1} &= \frac{q_k + q_{k+1}}{2}. \end{aligned} \tag{60}$$

Since the objective function is concave, by Jensen's inequality, the new policy strictly increases the objective. Finally considering the case where $p_k < p_{k+1}, q_k > q_{k+1}$, we can construct another feasible policy,

$$\begin{aligned} \tilde{p}_k = p_k,\ \tilde{p}_{k+1} = p_{k+1}, \\ \tilde{q}_k = q_{k+1},\ \tilde{q}_{k+1} = q_k. \end{aligned} \tag{61}$$

The function R^{ub} with variables p, q, τ can be written as,

$$R^{ub}(p, q, \tau) = t \log_2 \left(1 + \left(\frac{1}{t} + \frac{p}{t^2}\right) f\right), \tag{62}$$

where $f \triangleq M - (M-1)\left(1 + \frac{q}{\tau\sigma^2}\right)^{\frac{-\tau}{M-1}}$, $t \triangleq 1 - \frac{\tau}{T}$ and $0 \leq \tau < T$. The second order partial derivative of $R^{ub}(p, q, \tau)$ is given by,

$$\frac{\partial^2 R^{ub}}{\partial p \partial q} = \frac{\frac{\partial f}{\partial q}}{t\left(1 + f/t + pf/t^2\right)^2}. \tag{63}$$

Since f is monotonic in q, (63) is positive. As $\frac{\partial^2 R^{ub}}{\partial p \partial q} > 0$, by the definition of derivative,

$$\begin{aligned} R^{ub}(p, q, \tau) + R^{ub}(p + \delta, q + \alpha, \tau) > \\ R^{ub}(p + \delta, q, \tau) + R^{ub}(p, q + \alpha, \tau)\,,\ \delta, \alpha > 0. \end{aligned} \tag{64}$$

Since (64) holds for all $0 \leq \tau < T$, we have

$$\begin{aligned} \tilde{R}^{ub}(p, q) + \tilde{R}^{ub}(q + \delta, q + \alpha) > \\ \tilde{R}^{ub}(p + \delta, q) + \tilde{R}^{ub}(p, q + \alpha)\,, \end{aligned} \tag{65}$$

where $\tilde{R}^{ub}$ is obtained by,

$$\tilde{R}^{ub}(p, q) = \max_{\tau}\ R^{ub}(p, q, \tau)\,. \tag{66}$$

Finally, using (61) and (65) we can see that the newly constructed policy strictly increases the objective.

F. Proof of Lemma 3

Let us assume that the transmission rates in the k-th and the $k+1$-th intervals are different, i.e., $\tilde{R}^{ub}(p_k, q_k) \neq \tilde{R}^{ub}(p_{k+1}, q_{k+1})$. Before the $k+1$-th interval, the energy in the buffers of TX and the RX are $\Delta_r \triangleq \sum_{i=1}^{k} e^r_i - L\sum_{i=1}^{k} q_i$ and $\Delta_t \triangleq \sum_{i=1}^{k} e^t_i - LT\sum_{i=1}^{k} p_i$, respectively. W.l.o.s, we assume that $\Delta_r \leq \Delta_t$. We can construct another feasible policy

$$\begin{aligned} \tilde{p}_k = p_k + \delta,\ \tilde{p}_{k+1} = p_{k+1} - \delta, \\ \tilde{q}_k = q_k + \delta,\ \tilde{q}_{k+1} = q_{k+1} - \delta, \end{aligned} \tag{67}$$

where δ is chosen such that $\delta < \Delta_r$ and $\tilde{q}_k < \tilde{q}_{k+1}$. Now, (67) can be written as

$$\begin{aligned} \tilde{p}_k = \alpha p_k + (1-\alpha)\, p_{k+1},\ \tilde{p}_{k+1} = (1-\alpha)\, p_k + \alpha p_{k+1}, \\ \tilde{q}_k = \alpha q_k + (1-\alpha)\, q_{k+1},\ \tilde{q}_{k+1} = (1-\alpha)\, q_k + \alpha q_{k+1}, \end{aligned} \tag{68}$$

where $\alpha = 1 - \delta/(q_{k+1} - q_k)$. Using Jensen's inequality

$$\sum_{j=k}^{k+1} \tilde{R}^{ub}(\tilde{p}_j, \tilde{q}_j) > \sum_{j=k}^{k+1} \tilde{R}^{ub}(p_j, q_j)\,, \tag{69}$$

which concludes the proof.

REFERENCES

[1] R. Gangula, D. Gesbert, and D. Gunduz, "Optimizing feedback in energy harvesting miso communication channels," in *IEEE GlobalSIP*, Austin, TX, Dec. 2013.

[2] A. Kansal, J. Hsu, S. Zahedi, and M. B. Srivastava, "Power management in energy harvesting sensor networks," *ACM Trans. Embed. Comput. Syst.*, vol. 6, no. 4, Sept. 2007.

[3] S. Sudevalayam and P. Kulkarni, "Energy harvesting sensor nodes: survey and implications," *IEEE Communications Surveys Tutorials*, vol. 13, no. 3, pp. 443–461, Mar. 2011.

[4] O. Ozel, K. Tutuncuoglu, J. Yang, S. Ulukus, and A. Yener, "Transmission with energy harvesting nodes in fading wireless channels: optimal policies," *IEEE JSAC*, vol. 29, no. 8, pp. 1732–1743, Sept. 2011.

[5] M. Antepli, E. Uysal-Biyikoglu, and H. Erkal, "Optimal packet scheduling on an energy harvesting broadcast link," *IEEE JSAC*, vol. 29, no. 8, pp. 1721–1731, Sept. 2011.

[6] J. Yang, O. Ozel, and S. Ulukus, "Broadcasting with an energy harvesting rechargeable transmitter," *IEEE Transactions on Wireless Communications*, vol. 11, no. 2, pp. 571–583, Feb. 2012.

[7] B. Devillers and D. Gunduz, "A general framework for the optimization of energy harvesting communication systems with battery imperfections," *Journal of Comm. and Nets*, vol. 14, no. 2, pp. 130–139, Apr. 2012.

[8] D. Gunduz and B. Devillers, "Two-hop communication with energy harvesting," in *CAMSAP*, San Juan, Puerto Rico, Dec. 2011.

[9] C. Huang, R. Zhang, and S. Cui, "Throughput maximization for the gaussian relay channel with energy harvesting constraints," *IEEE JSAC*, vol. 31, no. 8, pp. 1469–1479, Aug. 2013.

[10] O. Orhan, D. Gunduz, and E. Erkip, "Energy harvesting broadband communication systems with processing energy cost," *IEEE Transactions on Wireless Communications*, vol. 13, no. 11, pp. 6095–6107, Nov. 2014.

[11] A. Bodin and D. Gunduz, "Energy harvesting communication system with finite set of transmission rates," in *European Wireless (EW) Conference*, Barcelona, Spain, May 2014.

[12] D. Gunduz, K. Stamatiou, N. Michelusi, and M. Zorzi, "Designing intelligent energy harvesting communication systems," *IEEE Communications Magazine*, vol. 52, no. 1, pp. 210–216, Jan. 2014.

[13] D. Love, R. Heath, V. K. N. Lau, D. Gesbert, B. Rao, and M. Andrews, "An overview of limited feedback in wireless communication systems," *IEEE JSAC*, vol. 26, no. 8, pp. 1341–1365, Oct. 2008.

[14] H. Edmundson, *Bounds on the Expectation of a Convex Function of a Random Variable.* RAND Corporation, 1957.

[15] A. W. Marshall, I. Olkin, and B. C. Arnold, *Inequalities: Theory of majorization and its applications*. Springer, 2010.

[16] W. Santipach and M. Honig, "Optimization of training and feedback overhead for beamforming over block fading channels," *IEEE Trans on Information Theory,*, vol. 56, no. 12, pp. 6103–6115, Dec. 2010.

[17] M. Kobayashi, N. Jindal, and G. Caire, "Training and feedback optimization for multiuser MIMO downlink," *IEEE Transactions on Communications*, vol. 59, no. 8, pp. 2228–2240, Aug. 2011.

[18] C. K. Au-Yeung and D. Love, "On the performance of random vector quantization limited feedback beamforming in a MISO system," *IEEE Transactions on Wireless Commm*, vol. 6, no. 2, pp. 458–462, Feb. 2007.

[19] N. Jindal, "MIMO broadcast channels with finite-rate feedback," *IEEE Trans on Inf. Theory*, vol. 52, no. 11, pp. 5045–5060, Nov. 2006.

[20] S. Boyd and L. Vandenberghe, *Convex optimization*. New York, NY, USA: Cambridge University Press, 2004.

[21] C. K. Ho and R. Zhang, "Optimal energy allocation for wireless communications with energy harvesting constraints," *IEEE Transactions on Signal Processing*, vol. 60, no. 9, pp. 4808–4818, Sept. 2012.

[22] M. A. Zafer and E. Modiano, "A calculus approach to energy-efficient data transmission with quality-of-service constraints," *IEEE/ACM Trans. Netw.*, vol. 17, no. 3, pp. 898–911, Jun. 2009.

[23] O. Ozel and S. Ulukus, "Achieving AWGN capacity under stochastic energy harvesting," *IEEE Transactions on Information Theory*, vol. 58, no. 10, pp. 6471–6483, Oct. 2012.

[24] S. Reddy and C. Murthy, "Dual-stage power management algorithms for energy harvesting sensors," *IEEE Trans on Wireless Comm*, vol. 11, no. 4, pp. 1434–1445, Apr. 2012.

[25] "Solar Resource and Meteorological Assessment Project (SOLRMAP)," `http://www.nrel.gov/midc/lmu/`.

Rajeev Gangula obtained the M.Tech degree from Indian Institute of Technology, Guwahati in June 2010 specializing in Signal processing. He obtained the M.Sc degree from Télécom ParisTech (EURECOM) in 2011. He is awarded Orange-MEEA scholarship for the M.Sc studies. He is currently a Ph.D student at EURECOM. His research interests lie in the areas of optimization and communication theory.

David Gesbert (F'11) is Professor and Head of the Mobile Communications Department, EURECOM, France. He obtained the Ph.D degree from Ecole Nationale Superieure des Telecommunications, France, in 1997. From 1997 to 1999 he has been with the Information Systems Laboratory, Stanford University. In 1999, he was a founding engineer of Iospan Wireless Inc, San Jose, Ca.,a startup company pioneering MIMO-OFDM (now Intel). D. Gesbert has published about 230 papers and several patents all in the area of signal processing, communications, and wireless networks. He was named in the 2014 Thomson-Reuters List of Highly Cited Researchers in Computer Science.

D. Gesbert was a co-editor of several special issues on wireless networks and communications theory, for JSAC (2003, 2007, 2009), EURASIP Journal on Applied Signal Processing (2004, 2007), Wireless Communications Magazine (2006). He authored or co-authored papers winning the 2012 SPS Signal Processing Magazine Best Paper Award, 2004 IEEE Best Tutorial Paper Award (Communications Society), 2005 Young Author Best Paper Award for Signal Proc. Society journals, and paper awards at conferences 2011 IEEE SPAWC, 2004 ACM MSWiM workshop. He co-authored the book "Space time wireless communications: From parameter estimation to MIMO systems", Cambridge Press, 2006.

Deniz Gündüz (S'03-M'08-SM'13) received the B.S. degree in electrical and electronics engineering from METU, Turkey in 2002, and the M.S. and Ph.D. degrees in electrical engineering from NYU Polytechnic School of Engineering in 2004 and 2007, respectively. After his PhD he served as a postdoctoral research associate at the Department of Electrical Engineering, Princeton University, and as a consulting assistant professor at the Department of Electrical Engineering, Stanford University. Since September 2012 he is a Lecturer in the Electrical and Electronic Engineering Department of Imperial College London, UK. Previously he was a research associate at CTTC in Barcelona, Spain. He also held a visiting researcher position at Princeton University from November 2009 until November 2011.

Dr. Gunduz is an Associate Editor of the IEEE TRANSACTIONS ON COMMUNICATIONS, and served as a guest editor of the EURASIP Journal on Wireless Communications and Networking, Special Issue on Recent Advances in Optimization Techniques in Wireless Communication Networks. He is the recipient of a Marie Curie Fellowship awarded by the European Commission, and a recipient of the Best Student Paper Award at the 2007 IEEE International Symposium on Information Theory (ISIT).

He is serving as a co-chair of the IEEE Information Theory Society Student Committee. He is also the co-director of the Imperial College Probability Center. He has served as the co-chair of the Network Theory Symposium at the 2013 and 2014 IEEE Global Conference on Signal and Information Processing (GlobalSIP), and he was a co-chair of the 2012 IEEE European School of Information Theory (ESIT). His research interests lie in the areas of communication theory and information theory with special emphasis on joint source-channel coding, multi-user networks, energy efficient communications and privacy.